

Article

Solution-Processed Titanium Oxide for Rear Contact Improvement in Heterojunction Solar Cells

Yu-Tsu Lee ¹, Fang-Ru Lin ¹ and Zingway Pei ^{1,2,3,*} 

¹ Department of Electrical Engineering, National Chung Hsing University, Taichung 40227, Taiwan; bill90867@hotmail.com (Y.-T.L.); ginkgo0518@hotmail.com (F.-R.L.)

² Graduate Institute of Optoelectronic Engineering, National Chung Hsing University, Taichung 40227, Taiwan

³ Innovation and Development Center of Sustainable Agriculture, National Chung Hsing University, Taichung 40227, Taiwan

* Correspondence: Zingway@dragon.nchu.edu.tw; Tel.: +886-4-2258-1549

Received: 7 August 2020; Accepted: 3 September 2020; Published: 7 September 2020



Abstract: In this work, we demonstrated a heterojunction Si solar cell utilizing chemically grown titanium oxide (TiO_x) as an electron-selective contact layer at its rear surface. With TiO_x, the rear surface was passivated to reduce carrier recombination. The reverse saturation current, which is an indicator of carrier recombination, exhibited a 4.4-fold reduction after placing a TiO_x layer on the rear surface. With reduced recombination, the open-circuit voltage increased from 433 mV to 600 mV and consequently, the power conversion efficiency (PCE) increased from 9.57 to 14.70%. By X-ray photoemission spectroscopy, the surface passivation was attributed to a silicon oxide interfacial layer formed during the chemical growth process. This passivation results in a 625 cm/s surface recombination velocity for the TiO_x-passivated Si surface, which is 2.4 times lower than the sample without TiO_x, ensuring the carriers pass through the rear contact without extensive recombination. According to these results, the band alignment for the heterojunction solar cell with and without a TiO_x rear contact layer was plotted, the reduced interfacial recombination and the electron and hole blocking structure are the main reasons for the observed efficiency enhancement.

Keywords: titanium oxide; electron-selective; chemical grown; surface passivation; heterojunction solar cell

PACS: J0101

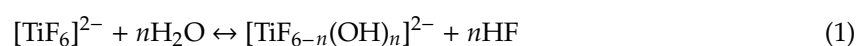
1. Introduction

With appropriate band alignment to Si, the sub-stoichiometric transition metal oxides (TMOs) [1], such as titanium oxide (TiO_x) [2–4], molybdenum oxide (MoO_x) [5], and nickel oxide (NiO_x) [6], have been investigated as either an electron-selective or a hole-selective contact in silicon solar cells. Conventionally, the ohmic contacts in Si were fabricated by depositing metals on a heavily-doped region, which is expensive and complex for Si solar cells. These TMO materials, generally deposited by either liquid phase deposition, thermal evaporation, or magnetron sputtering, exhibiting Ohmic contact in low resistance by appropriate band alignment, involve low temperature and low-cost processes. For example, a thin MoO_x film could be used to replace the boron-doped a-Si:H in a SHJ solar cell to achieve 22.5% PCE by improving short-circuit current density (J_{sc}) [7]. Due to its high valence-band energy, a TiO_x film demonstrated a large valence-band offset (~2.0 eV) to silicon forming a hole-blocking interface [8]. At the same time, the conduction band energy of TiO_x is similar to the Si, enabling electrons to pass through with effect-less barrier, as an electron-selective contact. Therefore, by using a TiO_x hole blocking contact, a silicon solar cell that exhibits a PCE of 11.2% could

be obtained [9]. However, those studies generally focus on the ability of replacing the front layer by an electron-selective TiO_x one, but rarely on the rear contact properties. Furthermore, in addition to electron-selectivity, the ability of interface passivation is also important to obtain high open-circuit voltages and high fill factors in a silicon solar cell. In this work, we utilize a full-area electron-selective TiO_x layer grown by liquid phase deposition (LPD) as a rear contact of Si to achieve high-efficiency. LPD is a fully chemical growth process, allowing the TiO_x layer to be grown uniformly. The ability for rear surface passivation was studied by examining the reverse saturation current, which is an indicator of carrier recombination in a junction diode. The advantage of rear surface passivation was explored by the external quantum efficiency at long wavelength. The origin of passivation was observed by X-ray photoemission spectroscopy and attributed to the formation of silicon oxide at the Si surface. The small surface recombination velocity that was calculated by minority carrier lifetime, ensures the carriers pass through the contact without extensive recombination.

2. Experimental Procedures

To fabricate the proposed solar cell, an n-type, 175 μm thick surface polished crystalline (100) silicon wafer (0.5–1 $\Omega\text{-cm}$) was used as substrate. Prior to deposition, the Si substrate was textured in a potassium hydroxide (KOH) solution and etched in an etchant solution ($\text{HF}:\text{H}_2\text{O} = 1:10$) for 30 sec to remove surface damage and then rinsed with deionized water. After cleaning, a thin layer of intrinsic a-Si:H (5 nm) and B-doped a-Si:H (20 nm) are deposited sequentially by plasma-enhanced chemical vapor deposition (13.56 MHz). A 80 nm thick indium-tin oxide (ITO) transparent conductor was then deposited by sputtering. After that, the front surface was passivated with photoresist for rear-side TiO_x deposition. The TiO_x was deposited in 8, 16, and 25 nm thicknesses by a LPD method, details of which were published previously [2,3]. $(\text{NH}_4)_2\text{TiF}_6$ solution and H_3BO_3 were used as precursors. To ensure a saturated concentration of TiO_x , TiO_x powders were added to the precursor. The deposition temperature was maintained at 40 $^\circ\text{C}$. The concentrations of $(\text{NH}_4)_2\text{TiF}_6$ and H_3BO_3 were 0.2 M and 0.6 M, respectively, in deionized water. The growth of TiO_2 consists of two equilibrium reactions. In the first step, the TiF ligand interacts with H_2O to form a titanium hydroxyl complex and HF (Equation (1)). The titanium hydroxyl complex is further transformed into TiO_x through a dehydration reaction. To maintain the continuous growth of TiO_x , the first equation should work forward by reducing the concentration of F ion simultaneously. This was achieved by the reaction of H_3BO_3 with HF in the second step (Equation (2)) [10,11]:



In this step, the chemical reaction consumes uncoordinated F to form stable BF_4^- ions. Therefore, the consumption of the HF drives the chemical reaction represented in the Equation (1) toward TiO_x deposition on the substrate by dissolving supersaturated TiO_2 powder in the solution, in order to balance the chemical reaction. After TiO_x deposition, the photoresist was removed. The front (Ag~100 nm) and back contact (Al~200 nm) were deposited sequentially by a thermal evaporator through a shadow mask. The schematic diagram of the resulting solar cell device is shown in Figure 1a. To analyse the device, the dark current density voltage (I-V) characteristics were measured by a B2912A semiconductor parameter analyzer (Agilent, Santa Clara, CA, USA) on a probe station. The photovoltaic characteristics were measured by a calibrated solar simulator under AM1.5 G (100 mW/cm^2) conditions. A QE-3000 system (Titan Electro-Optics, Taipei, Taiwan) was used to obtain external quantum efficiency (EQE). To study the material properties, a transmission electron microscope (TEM, model JEM-2100F, JEOL, Tokyo, Japan) was used to explore the TiO_x/Si interfaces. X-ray Photoelectron Spectroscopy (XPS, model PHI 5000 Versa Probe, ULVAC-PHI, Kanagawa, Japan) was used to understand the microstructure of TiO_x on Si. The lifetime was measured by a WCT-120 system (Sinton, Boulder,

CO, USA) in quasi-steady-state photoconductance mode. The surface recombination velocity was calculated from the obtained lifetime.

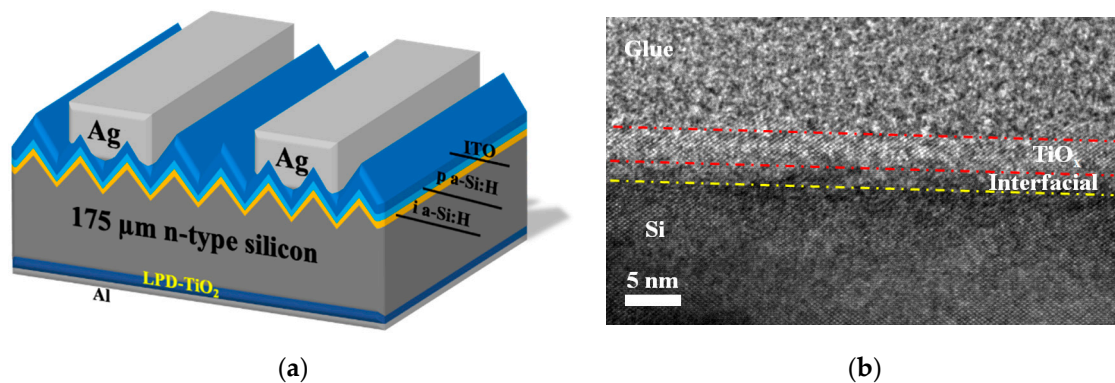


Figure 1. (a) The schematic diagram of the fabricated heterojunction solar cell that exhibits an LPD-grown interfacial layer between Al and Si at its rear surface. (b) TEM images of thin TiO_x layer on the Si surface. The sample TiO_x layer was grown uniformly on the Si surface.

3. Results and Discussions

A TEM image of the TiO_x/Si interface is shown in Figure 1b. To grow a thin TiO_x layer, the growth rate is the key factor in the LPD process. The growth rate was determined by the thickness measurement on a thicker TiO_x by SEM. The TiO_x was then grown to the designed thickness by controlling the time in the LPD process. In Figure 1b, the designed thickness is 5 nm. From the figure, the interfacial and TiO_x layers are approximately 1 and 4 nm thick, as indicated. The measured thickness is consistent with the designed thickness, therefore, the thickness used in the device indicates matches the design thickness. The dark and photo-current density to voltage characteristics (J-V) are illustrated in Figure 2a,c, respectively. Without solar light illumination, both solar cell devices with and without a TiO_x rear contact layer exhibit normal pn-junction diode behavior. The solar cell without TiO_x rear contact layer exhibits a higher current density for the same applied voltage. This implies the carriers are injected into device much easier without a TiO_x rear contact layer, however, the ease of injection also indicates the possibility of a smaller open-circuit voltage (V_{oc}), in which the V_{oc} is determined as the voltage at which the solar generation current and the injected current are balanced. The ideality factor, n , of both devices was calculated and is shown in Figure 2b by the following pn-junction diode equations, as shown in Equation (3):

$$J = J_0 \left(\exp\left(\frac{qV}{nkT}\right) - 1 \right) \quad (3)$$

in which J is the diode current, J_0 is the reverse saturation current density, q is the electric charge of electron, k is the Boltzman constant, T is the absolute temperature, V is the applied voltage and the n is the ideality factor. The term n generally accounts for recombination at either the bulk or junctions, the heterointerfaces, and contact resistance under forward-biased conditions [12]. The calculated ideality factor for a solar cell without a TiO_x rear contact layer is approximately 1.73 at a voltage smaller than 0.45 V and it increases rapidly after 0.45 V. In comparison, the solar cell with a 8 nm thick TiO_x rear contact layer exhibits a higher ideality factor, approximately 2.3, at voltages smaller than 0.55 V and a slight increase after this voltage. Since the bulk and the front contacts are identical for both solar cells, the difference in ideality factor must be caused by the rear contact, either from rear interface recombination or due to the interfacial barrier provided by TiO_x. The rapidly increased ideality factor at voltages higher than 0.45 V indicates a high voltage-drop in this region that may be attributed to high interfacial states for recombination in solar cells without a TiO_x rear contact layer. This could be clarified by the reverse saturation current, J_0 , under reversed biased conditions, in which the J_0 contains information of the generation and recombination processes in the entire device. The reverse saturation current density, J_0 , for a reference device (without TiO_x) is 1.1×10^{-7} A/cm², and it is 2.5×10^{-8} A/cm²

for a device with a TiO_x rear contact layer. The solar cell device with TiO_x exhibits approximately a 4.4-fold reduction. These findings indicate that insertion of a thin layer of TiO_x may passivate the density of states of Si on the rear surface and improve the electrical contact behavior.

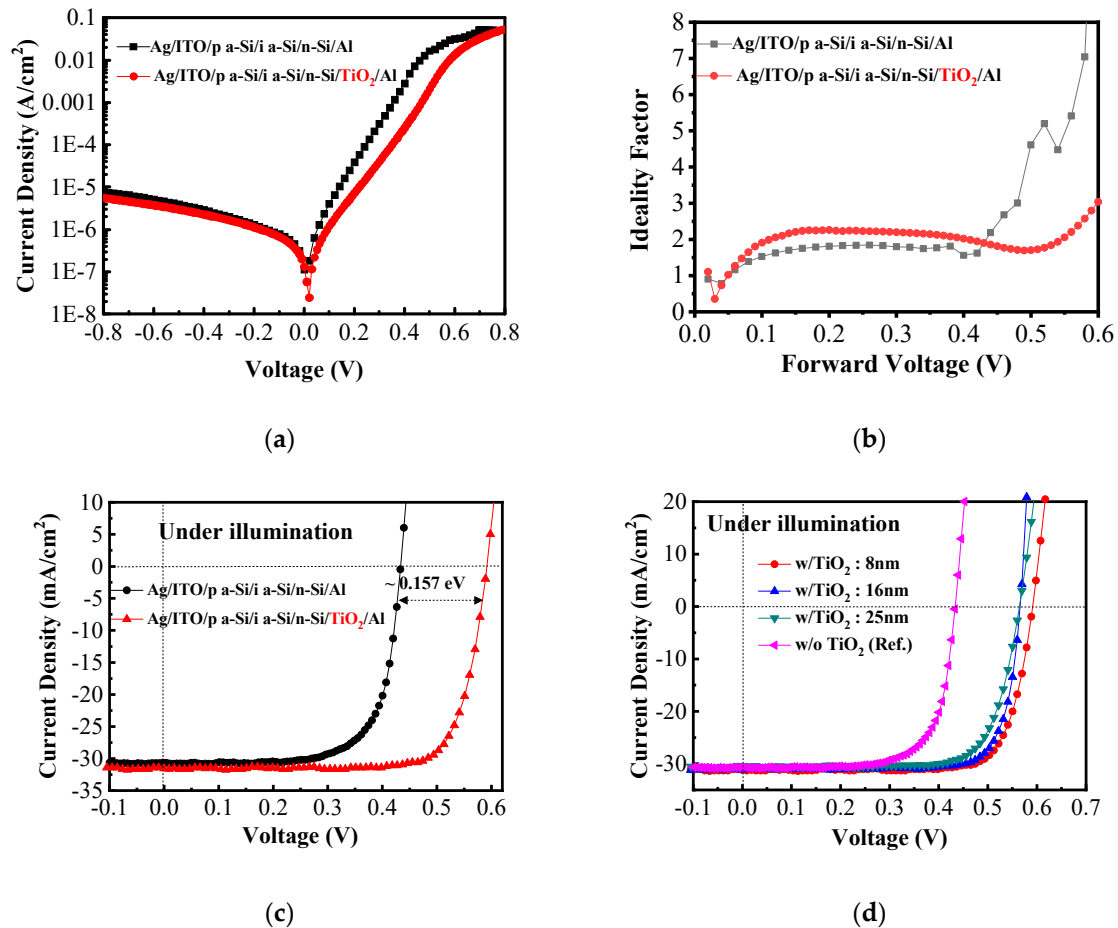


Figure 2. (a) The diode current density–voltage characteristics for the solar cell without and with 8 nm thick TiO_x rear contact layer at dark environment. (b) The ideality factor that calculated from the diode characteristics. (c) The diode current density–voltage characteristics for the solar cell without and with 8 nm thick TiO_x rear contact layer under solar simulator illumination. (d) The diode current density–voltage characteristics for the solar cell without and with a TiO_x rear contact layer of different thickness under solar simulator illumination.

The photocurrent–voltage characteristics of the TiO_x and referenced solar cells are illustrated in Figure 2c. The short-circuit current density (J_{sc}), fill factor (FF) and open-circuit voltage (V_{oc}) of a solar cell with an 8 nm TiO_x rear interfacial layer are 31.5 mA/cm^2 , 0.778, and 0.6 V, respectively. As a consequence, a power conversion efficiency (PCE) of 14.70% is achieved. Without a TiO_x rear contact, the values of those solar cell performance indicators are 30.7 mA/cm^2 , 0.716, and 0.43 V, yielding an PCE of 9.57%. With the increased thickness of TiO_x (16 and 25 nm), the V_{oc} of devices decreased slightly, as compared to the solar cell device with a 8 nm thick TiO_x rear contact layer. The PCE was reduced slightly to 13.81 and 12.96%, respectively. The details of the V_{oc} , J_{sc} , FF, PCE, series resistance (R_s) and shunt resistance (R_{sh}) for the solar cell devices are listed in Table 1.

Table 1. Photovoltaic characteristics of the TiO_x/Si heterojunction SOLAR CELLS.

Parameter	V _{oc} (mV)	J _{sc} (mA/cm ²)	Fill Factor	PCE (%) ^b	R _s (Ω-cm ²)	R _{sh} (Ω-cm ²)
Ref. ^a	433	30.7	0.716	9.57	2.59	1562
8 nm	600	31.5	0.778	14.70	2.46	1244
16 nm	566	30.9	0.790	13.81	1.89	1564
25 nm	564	30.4	0.756	12.96	3.67	776

^a p-a-Si:H/n-Si solar cell; ^b Power Conversion Efficiency (PCE).

The enhancement in the V_{oc} for the TiO_x device is consistent with the higher ideality factor at forward-biased and the low recombination current density under reverse-biased conditions given by the following expression:

$$V_{oc} = \frac{nkT}{q} \ln \left(\frac{J_{sc}}{J_0} + 1 \right) \quad (4)$$

According to this equation, a high ideality factor and low recombination current density will result in a high V_{oc} if the photocurrent density remains constant. In contrast to V_{oc}, the J_{sc} is similar for devices with and without TiO_x. They show only a slight difference, which is 0.7 mA/cm². The EQE for these two devices was taken at wavelengths from 400 to 1200 nm to understand the origin of the J_{sc} enhancement, as shown in Figure 3. The EQE for both devices are almost identical before 800 nm. After this wavelength, the device with TiO_x shows a slight enhancement. The enhancement ratio was calculated and is displayed in the lower part of Figure 3. The enhancement is increased around 20% at wavelengths near 1100 nm. Usually long wavelength incident light can reach the rear side of a Si solar cell because of the low absorption coefficient at these wavelengths. Therefore, the enhancement in the EQE is attributed to the formation of TiO_x at the rear contact that passivates the interfaces. The microstructure of the TiO_x and Si interface will be discussed later using an XPS investigation. In addition to the interface passivation, the valence band edge of the TiO_x samples are higher than the edge of the valence band of the Si from our previous study, as the TiO_x will repel photogenerated holes back to the front contact, which increases the J_{sc} and EQE.

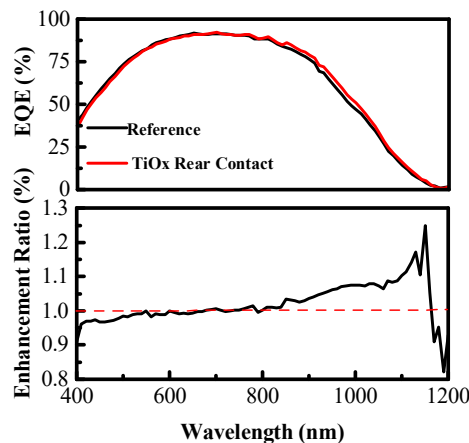
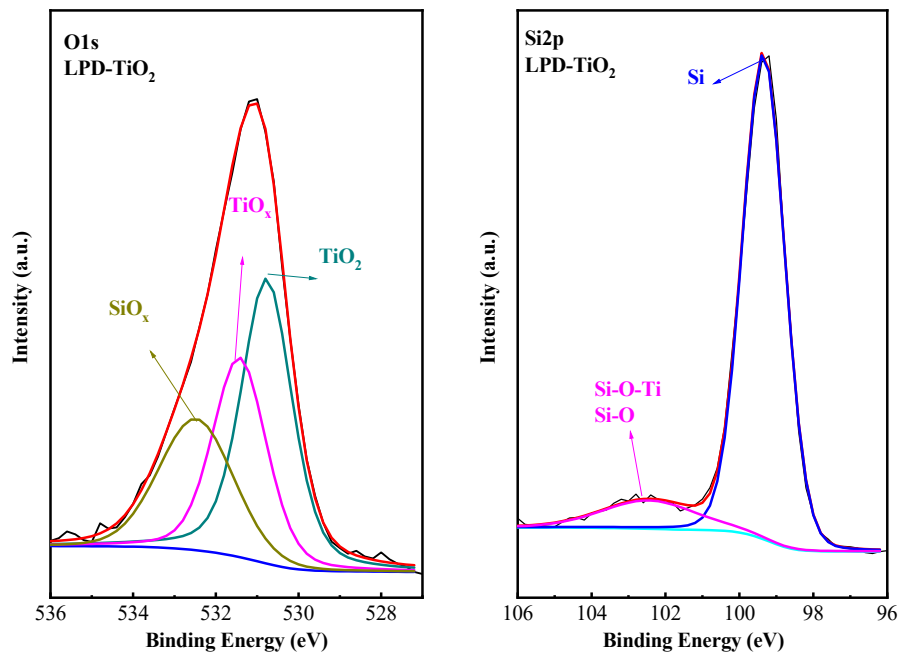


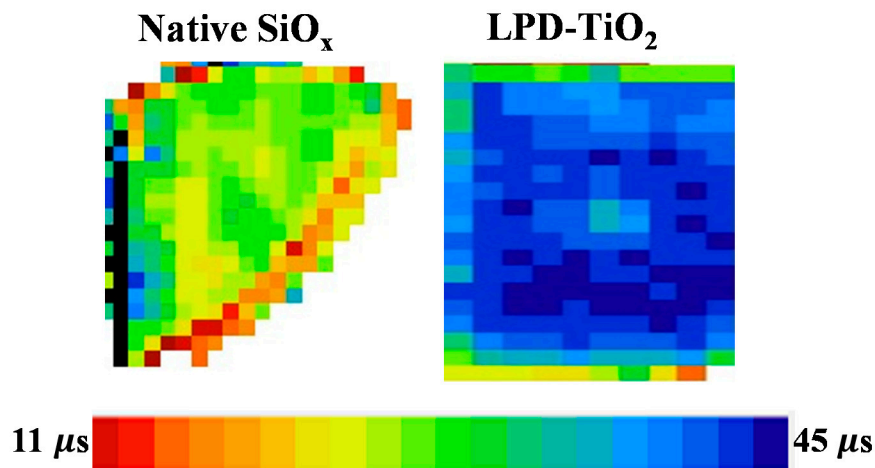
Figure 3. The external quantum efficiency (EQE) for the solar cells with and without a TiO_x rear contact layer at wavelengths ranging from 400 to 1200 nm (**upper**). Enhancement of EQE for the solar cells with and without TiO_x rear contact layer calculated from the EQE spectrum (**lower**).

Figure 4a depicts the O_{1s} and Si_{2p} core-level microstructure of the TiO_x obtained according to the XPS results. The O_{1s} spectrum exhibits three peaks after deconvolution, which correspond to TiO₂ (530.7 eV), oxygen deficient TiO_x (531.4 eV) and SiO_x (532.5 eV) [13–15]. The Si-bonded O signal covers a broad energy range, that overlaps with the oxygen-deficient TiO_x signal, indicating the existence of oxygen deficient SiO_x and cross-bonding, such as Si-O-Ti. The Si 2p signal has two peaks, corresponding to Si (99 eV) and Si-O (102 eV), respectively [16]. The appearance of Si-O bonding

reveals a small amounts of silicon oxide exists either in the TiO_x or at the Si surface. The formation of SiO_x is a natural result in the LPD process. Water will react with the Si surface to form the oxide naturally. The HF will further dissolve SiO_2 into solution by etching. Finally, the dissolved SiO_2 and TiO_2 will regrow on the native oxide to form a layer comprising SiO_x , TiO_x and TiO_2 .



(a)



(b)

Figure 4. (a) The O_{1s} and Si_{2p} core-level microstructure of the TiO_x/Si obtained by XPS. (b) The images of the minority carrier lifetime for Si surfaces without (covered by native oxide) and with TiO_x passivation.

The reduction in the dark current density provides evidence of improved junction quality. The formation of the SiO_x between Si and TiO_x could passivate the interfaces reducing the recombination. The physical evidence is the reduction of the surface recombination velocity (S). The SRV could be

derived by the minority carrier lifetime (τ). The relationship of S and τ could be expressed by the following equation [17,18]:

$$\frac{1}{\tau} = \frac{1}{\tau_b} + \frac{2S}{W} \quad (5)$$

in which the τ is the minority carrier lifetime by measurement, τ_b is the averaged bulk lifetime, S is the surface recombination velocity to be calculated, and W is the wafer thickness. The minority carrier lifetime for the bare-Si (with native oxide) and TiO_x -grown Si are indicated at Figure 4b. The bare-Si and TiO_x -grown Si had average lifetimes of 16.8 and 40 μs , respectively. To calculate the S , the bulk lifetime was assumed to be 19 ms [19]. The S values were 625 and 1488 cm/s for TiO_x and native oxide grown Si surface, respectively, by calculation. The TiO_x exhibits a 2.4-fold reduction of the surface recombination velocity compared to native oxide on Si. As a consequence, the TiO_x/Si has better passivation ability than native oxide.

The band alignments of the proposed device structure are plotted at Figure 5a,b for the heterojunction (HJ) solar cell with and without a TiO_x rear contact layer, respectively. The conduction band edge (E_C) and valence band edge (E_V), for the Si (100) are 4.01 eV and 5.17 eV below the vacuum level, respectively. The Fermi energy (E_F) of the n-type Si is calculated according to the doping concentration (resistivity $\sim 0.5 \Omega\text{-cm}$), which is 4.22 eV. The titanium oxide with empty and filled band edges at 4 eV and 7.2 eV below the vacuum level, respectively. Furthermore, the Fermi energy of the LPD- TiO_x layer is 4.2 eV [3]. The conduction band and valence edges are 3.9~4.0 and 5.6~5.7 eV for amorphous silicon (a-Si:H) adopted from literature [20,21]. The band gap of a-Si:H is assumed to be ~ 1.7 eV [22]. With heavy B-doping, the a-Si:H film has a work function of 4.9 eV.

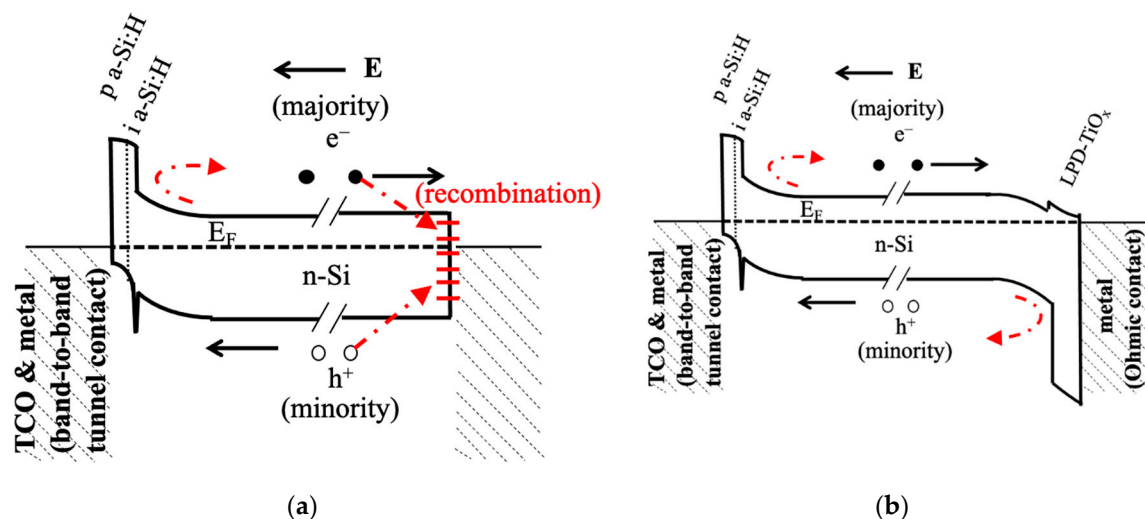


Figure 5. The schematic band alignment for the Si heterojunction solar cell (a) without and (b) with a chemically grown TiO_x rear contact layer. The electron- and hole- blocking were plotted.

In both device structures, the B-doped a-Si:H film can be used as an electron blocking layer to push electrons moving from the anode to the cathode preventing electron recombination at the p-type doping region. Meanwhile, the holes could be collected by the anode despite a “spike” barrier. However, the alignment is quite different for the rear contact. The grown of a thin TiO_x layer between Si and the contact metal offers two advantages. One is the building of a hole blocking layer that prevents holes from recombining at the cathode side. The other contribution is the passivation of defects at Si/Al interfaces. One suggestion is the formation of AlO_x at interfaces [23]. The Al atoms have a large oxygen affinity that easily attracts oxygen atoms from the TiO_x interlayer to form an interfacial AlO_x layer by a redox reaction after annealing. This interfacial AlO_x layer is assumed to be a nonstoichiometric Al-rich layer that accounts for the low contact resistivity obtained for these devices. However, this cannot be clarified in our structure, as Al/ TiO_x interfaces cannot be studied

because the thin TiO_x layer is grown underneath a thick Al layer. On the other hand, the growth of titanium oxide on the Si surface by a liquid phase method with oxygen-containing precursors also induces the growth of oxide at interfaces. The composition of the TiO_2 layer is highly oxygen-deficient TiO_{2-x} and contains a SiO_x interfacial layer in our experiments. The high oxygen deficiency reveals that LPD TiO_x exhibits high conductivity due to the free electron generation by oxygen vacancies [6]. Therefore, the contact resistivity at the Si/ TiO_x interface is small due to the higher conductivity and hence the cell's FF improves [7]. The formation of the interfacial Si oxide will passivate the Si surface, as understood from the X-ray photoemission spectroscopy results.

4. Conclusions

In conclusion, we have demonstrated a metal-oxide/Si heterojunction solar cell utilizing a low temperature liquid phase process-grown titanium oxide layer. With a rear interface engineering TiO_x layer, a power conversion efficiency of 14.70% is achieved, a 9.57% enhancement. The reduction of carrier recombination at the rear surface causes this enhancement by improving the open-circuit voltage from 433 to 600 mV. The formation of interfacial Si oxide and the increased minority carrier lifetime from 16.8 to 40 ms, imply the interface between Al and Si was well-passivated. In addition, the formation of TiO_x at the rear surface also cause a hole-blocking behavior that enhances the short-circuit current and partially reduces the recombination. As a consequence, chemically grown titanium oxide is suitable for application in high performance, low cost Si solar cells.

Author Contributions: Y.-T.L. and Z.P. designed the experiments; F.-R.L. performed the experiments; Y.-T.L. and Z.P. analyzed the data; Y.-T.L. and Z.P. wrote the paper. All authors have read and agreed to the published version of the manuscript.

Funding: This research was funded by Ministry of Science and Technology of (MOST) Taiwan under grant MOST 108-2221-E-005-061-, MOST 108-2638-E-005-001-MY2, MOST 109-2218-E-005-012- and Ministry of Education, Taiwan, R.O.C. under Higher Education Sprout Project. And the APC was founded by MOST 108-2638-E-005-001-MY2.

Conflicts of Interest: The authors declare no conflict of interest.

References

1. Meyer, J.; Hamwi, S.; Kröger, M.; Kowalsky, W.; Riedl, T.; Kahn, A. Transition Metal Oxides for Organic Electronics: Energetics, Device Physics and Applications. *Adv. Mater.* **2012**, *24*, 5408–5427. [[CrossRef](#)]
2. Lee, Y.-T.; Lin, F.-R.; Chen, C.-H.; Pei, Z. A 14.7% Organic/Silicon Nanoholes Hybrid Solar Cell via Interfacial Engineering by Solution-Processed Inorganic Conformal Layer. *ACS Appl. Mater. Interfaces* **2016**, *8*, 34537–34545. [[CrossRef](#)]
3. Lee, Y.-T.; Lin, F.-R.; Lin, T.-C.; Chen, C.-H.; Pei, Z. Low-Temperature, Chemically Grown Titanium Oxide Thin Films with a High Hole Tunneling Rate for Si Solar Cells. *Energies* **2016**, *9*, 402. [[CrossRef](#)]
4. Lee, C.; Bae, S.; Park, H.; Choi, D.; Song, H.; Lee, H.; Ohshita, Y.; Kim, D.; Kang, Y.; Lee, H.-S. Properties of Thermally Evaporated Titanium Dioxide as an Electron-Selective Contact for Silicon Solar Cells. *Energies* **2020**, *13*, 678. [[CrossRef](#)]
5. Battaglia, C.; Yin, X.; Zheng, M.; Sharp, I.D.; Chen, T.; McDonnell, S.; Azcatl, A.; Carraro, C.; Ma, B.; Maboudian, R.; et al. Hole Selective MoOx Contact for Silicon Solar Cells. *Nano Lett.* **2014**, *14*, 967–971. [[CrossRef](#)]
6. Islam, R.; Shine, G.; Saraswat, K.C. Schottky barrier height reduction for holes by Fermi level depinning using metal/nickel oxide/silicon contacts. *Appl. Phys. Lett.* **2014**, *105*, 182103. [[CrossRef](#)]
7. Geissbühler, J.; Werner, J.; Martin de Nicolas, S.; Barraud, L.; Hessler-Wyser, A.; Despeisse, M.; Nicolay, S.; Tomasi, A.; Niesen, B.; De Wolf, S.; et al. 22.5% efficient silicon heterojunction solar cell with molybdenum oxide hole collector. *Appl. Phys. Lett.* **2015**, *107*, 081601. [[CrossRef](#)]
8. Avasthi, S.; McClain, W.E.; Man, G.; Kahn, A.; Schwartz, J.; Sturm, J.C. Hole-blocking titanium-oxide/silicon heterojunction and its application to photovoltaics. *Appl. Phys. Lett.* **2013**, *102*, 203901. [[CrossRef](#)]

9. Nagamatsu, K.A.; Avasthi, S.; Sahasrabudhe, G.; Man, G.; Jhaveri, J.; Berg, A.H.; Schwartz, J.; Kahn, A.; Wagner, S.; Sturm, J.C. Titanium dioxide/silicon hole-blocking selective contact to enable double-heterojunction crystalline silicon-based solar cell. *Appl. Phys. Lett.* **2015**, *106*, 123906. [[CrossRef](#)]
10. Kishimoto, H.; Takahama, K.; Hashimoto, N.; Aoi, Y.; Deki, S. Photocatalytic activity of titanium oxide prepared by liquid phase deposition (LPD). *J. Mater. Chem.* **1998**, *8*, 2019–2024. [[CrossRef](#)]
11. Lee, M.-K.; Lee, H.-C.; Hsu, C.-M. High dielectric constant TiO₂ film grown on polysilicon by liquid phase deposition. *Mater. Sci. Semicond. Process.* **2007**, *10*, 61–67. [[CrossRef](#)]
12. Giebink, N.C.; Wiederrecht, G.P.; Wasielewski, M.R.; Forrest, S.R. Ideal diode equation for organic heterojunctions. I. Derivation and application. *Phys. Rev. B* **2010**, *82*, 155305. [[CrossRef](#)]
13. Fang, Q.; Meier, M.; Yu, J.J.; Wang, Z.M.; Zhang, J.Y.; Wu, J.X.; Kenyon, A.; Hoffmann, P.; Boyd, I.W. FTIR and XPS investigation of Er-doped SiO₂–TiO₂ films. *Mater. Sci. Eng. B* **2003**, *105*, 209–213. [[CrossRef](#)]
14. Xu, W.-X.; Zhu, S.; Fu, X.-C. XPS study of TiO_x thin films deposited on glass substrates by the sol–gel process. *Appl. Surf. Sci.* **1998**, *136*, 194–205. [[CrossRef](#)]
15. Erdem, B.; Hunsicker, R.A.; Simmons, G.W.; Sudol, E.D.; Dimonie, V.L.; El-Aasser, M.S. XPS and FTIR Surface Characterization of TiO₂ Particles Used in Polymer Encapsulation. *Langmuir* **2001**, *17*, 2664–2669. [[CrossRef](#)]
16. Pei, Z.; Hwang, H.L. Formation of silicon nano-dots in luminescent silicon nitride. *Appl. Surf. Sci.* **2003**, *212–213*, 760–764. [[CrossRef](#)]
17. Yu, P.; Tsai, C.-Y.; Chang, J.-K.; Lai, C.-C.; Chen, P.-H.; Lai, Y.-C.; Tsai, P.-T.; Li, M.-C.; Pan, H.-T.; Huang, Y.-Y.; et al. 13% Efficiency Hybrid Organic/Silicon-Nanowire Heterojunction Solar Cell via Interface Engineering. *ACS Nano* **2013**, *7*, 10780–10787. [[CrossRef](#)]
18. Dingemans, G.; Kessels, W.M.M. Status and prospects of Al₂O₃-based surface passivation schemes for silicon solar cells. *J. Vac. Sci. Technol. A* **2012**, *30*, 040802. [[CrossRef](#)]
19. Schmidt, J.; Aberle, A.G. Accurate method for the determination of bulk minority-carrier lifetimes of mono- and multicrystalline silicon wafers. *J. Appl. Phys.* **1997**, *81*, 6186–6199. [[CrossRef](#)]
20. Dao, V.A.; Heo, J.; Choi, H.; Kim, Y.; Park, S.; Jung, S.; Lakshminarayan, N.; Yi, J. Simulation and study of the influence of the buffer intrinsic layer, back-surface field, densities of interface defects, resistivity of p-type silicon substrate and transparent conductive oxide on heterojunction with intrinsic thin-layer (HIT) solar cell. *Sol. Energy* **2010**, *84*, 777–783. [[CrossRef](#)]
21. Pei, Z.; Thiyagu, S.; Jhong, M.-S.; Hsieh, W.-S.; Cheng, S.-J.; Ho, M.-W.; Chen, Y.-H.; Liu, J.-C.; Yeh, C.-M. An amorphous silicon random nanocone/polymer hybrid solar cell. *Sol. Energy Mater. Sol. Cells* **2011**, *95*, 2431–2436. [[CrossRef](#)]
22. Pei, Z.; Chang, S.; Liu, C.; Chen, Y. Numerical Simulation on the Photovoltaic Behavior of an Amorphous-Silicon Nanowire-Array Solar Cell. *IEEE Electron. Device Lett.* **2009**, *30*, 1305–1307.
23. Jeong, H.Y.; Lee, J.Y.; Choi, S.-Y.; Kim, J.W. Microscopic origin of bipolar resistive switching of nanoscale titanium oxide thin films. *Appl. Phys. Lett.* **2009**, *95*, 162108. [[CrossRef](#)]

